Spherical relativistic Hartree theory in a Woods-Saxon basis

Shan-Gui Zhou*
School of Physics, Peking University, Beijing 100871, China;
Max-Planck-Institut für Kernphysik, 69029 Heidelberg, Germany;
Institute of Theoretical Physics, Chinese Academy of Sciences, Beijing 100080, China;
and Center of Theoretical Nuclear Physics, National Laboratory of Heavy Ion Accelerator, Lanzhou 730000, China

Jie Meng†
School of Physics, Peking University, Beijing 100871, China;
Physikdepartment, Technische Universität München, 85748 Garching, Germany;
Institute of Theoretical Physics, Chinese Academy of Sciences, Beijing 100080, China;
and Center of Theoretical Nuclear Physics, National Laboratory of Heavy Ion Accelerator, Lanzhou 730000, China

P. Ring‡
Physikdepartment, Technische Universität München, 85748 Garching, Germany
(Received 12 March 2003; published 23 September 2003)

The Woods-Saxon (WS) basis is suggested to replace the widely used harmonic oscillator basis for solving the relativistic mean-field theory in order to generalize it to study exotic nuclei. As an example, the relativistic Hartree theory is solved for spherical nuclei in a Woods-Saxon basis obtained by solving either the Schrödinger equation or the Dirac equation (labeled as SRHSWS and SRHDWS, respectively, and SRHWS for both). In SRHDWS, the negative energy states in the Dirac sea must be properly included. The WS basis in SRHDWS could be smaller than that in SRHSWS, which will simplify the deformed problem. The results from SRHWS are compared in detail with those from solving the spherical relativistic Hartree theory in the harmonic oscillator basis (SRHHO) and those in the coordinate space (SRHR). All of these approaches give identical nuclear properties such as total binding energies and root mean square radii for stable nuclei. For exotic nuclei, e.g., ^{72}Ca, SRHWS satisfactorily reproduces the neutron density distribution from SRHR, while SRHHO fails. It is shown that the Woods-Saxon basis can be extended to more complicated situations for exotic nuclei where both deformation and pairing have to be taken into account.

DOI: 10.1103/PhysRevC.68.034323 PACS number(s): 21.60.−n, 21.10.Gv, 21.10.Dr

I. INTRODUCTION

The existence of an average field in an atomic nucleus revealed by the exceptional role of nuclear magic numbers provides the foundation of the nuclear shell model and various mean-field approaches [1–3]. This average field is believed to be approximated most closely by a Woods-Saxon (WS) potential [4], either by analyzing the radial dependence of the nuclear force or by deriving it from a microscopic two-body force.

Since eigenfunctions for the WS potential cannot be given analytically, as good approximations for stable nuclei, one often adopts the harmonic oscillator (HO) potential in shell model calculations for both spherical [1] and deformed nuclei [5] or the square well. The HO eigenfunctions also often serve as a complete basis in solving equations in both nonrelativistic and relativistic mean-field approximations such as the Skyrme Hartree-Fock (SHF), Hartree-Fock-Bogoliubov (HFB), relativistic Hartree (RH), and relativistic Hartree-Bogoliubov (RHB) theories. In these approaches, solutions of the corresponding equations are transformed into a matrix diagonalization problem which can be easily dealt with.

However, due to the incorrect asymptotic behavior of the HO wave functions, the expansion in a localized HO basis is not appropriate for the description of drip line nuclei [6–8], which display many interesting features because of the extremely weakly binding properties; that is, the coupling between bound states and the continuum due to pairing correlations, the large spatial density distribution or possible modifications of shell structure, etc. One must improve the asymptotic behavior of HO wave functions, e.g., by performing a local scaling transformation [9].

A proper representation for solving the HFB or RHB equations for drip line nuclei is in the coordinate space [7,10–12], where wave functions are approximated on a spatial lattice and the continuum is discretized by suitably large box boundary conditions. The HFB method solved in r space can take into account all the mean-field effects of the coupling to the continuum fully [6,7,10,13]. Nevertheless for deformed nuclei, working in r space becomes much more difficult and numerically very sophisticated [8]. Particularly, it becomes very time consuming when pairing correlations are included. Therefore, much effort is made towards a more efficient solution of the HFB or RHB equations, e.g., using natural orbitals [14] or working on basis-spline Galerkin lattices [15,16].

*Electronic address: sgzhou@mpi-hd.mpg.de; http://jcnp.pku.edu.cn/~sgzhou
†Electronic address: mengj@pku.edu.cn
‡Electronic address: ring@physik.tu-muenchen.de

A reconciler between the HO basis and r space may be the WS basis because (i) the WS potential represents the nuclear average field more suitably than the HO potential and (ii) in principle, there are no localization restrictions on the WS potential. Although analytical wave functions cannot be given for the WS potential, one may easily find numerical solutions for a spherical WS potential in r space by virtue of various effective methods of solving ordinary differential equations [17]. One can still use a large box boundary condition to discretize the continuum. These WS wave functions can thus be used as a complete basis for spherical or deformed systems, and one finally comes back to the familiar matrix diagonalization problem.

In the present work, we restrict the application of this method to nuclei with spherical symmetry, which largely facilitates the discussion of basic principles and allows one to present illustrations for the radial dependence of all relevant physical quantities such as density distributions. We combine this approach with the relativistic Hartree theory [18], which provides a framework for describing the nuclear many body problem as a relativistic system of baryons and mesons and, together with its extensions with deformation and/or pairing correlations included, has been successfully applied to the studies of nuclear matter and properties of finite nuclei throughout the periodic table [19,20].

The paper is organized as follows. In Sec. II, we give a brief reminder of the formalism of the relativistic Hartree theory. The numerical details of solving it in the WS basis are given in Sec. III. In Sec. IV, we present our results and compare them to those obtained in the HO basis and in r space. We also discuss the contribution from negative energy states in the Dirac sea in the same section. Finally, the work is summarized in Sec. V.

Throughout the paper, the relativistic Hartree theories solved in r space, in the HO basis, and in the WS basis are abbreviated as ''SRHR,'' ''SRHHO,'' and ''SRHWS,'' where the first ''S'' represents ''spherical.'' We use ''SWS'' and ''DWS'' to distinguish the WS basis which is obtained from solving the Schrödinger equation or the Dirac equation with initial WS potentials, respectively. Thus we have SRHSWS and SRHDWS theories.

II. BASIC FORMALISM OF THE RELATIVISTIC HARTREE THEORY

The starting point of the relativistic Hartree theory is a Lagrangian density where nucleons are described as Dirac spinors which interact via the exchange of several mesons (σ, ω, and ρ) and the photon [18–20],

$$\begin{aligned}\mathcal{L}=&\bar{\psi}_i(i\not\partial-M)\psi_i+\frac{1}{2}\partial_\mu\sigma\partial^\mu\sigma-U(\sigma)-g_\sigma\bar{\psi}_i\sigma\psi_i\\&-\frac{1}{4}\Omega_{\mu\nu}\Omega^{\mu\nu}+\frac{1}{2}m_\omega^2\omega_\mu\omega^\mu-g_\omega\bar{\psi}_i\not\omega\psi_i-\frac{1}{4}\vec{R}_{\mu\nu}\vec{R}^{\mu\nu}\\&+\frac{1}{2}m_\rho^2\vec{\rho}_\mu\vec{\rho}^\mu-g_\rho\bar{\psi}_i\not\vec{\rho}\vec{\tau}\psi_i-\frac{1}{4}F_{\mu\nu}F^{\mu\nu}\\&-e\bar{\psi}_i\frac{(1-\tau_3)}{2}\not A\psi_i,\end{aligned}\tag{1}$$

where the summation convention is used and the summation over i runs over all nucleons, $\not x\equiv\gamma^\mu x_\mu=\gamma_\mu x^\mu$, M the nucleon mass, and m_σ, g_σ, m_ω, g_ω, m_ρ, g_ρ are the masses and coupling constants of the respective mesons. Isovector quantities are indicated by over arrows. The nonlinear self-coupling for the scalar mesons is given by [21]

$$U(\sigma)=\frac{1}{2}m_\sigma^2\sigma^2+\frac{g_2}{3}\sigma^3+\frac{g_3}{4}\sigma^4,\tag{2}$$

and field tensors for the vector mesons and the photon fields are defined as

$$\begin{aligned}\Omega_{\mu\nu}&=\partial_\mu\omega_\nu-\partial_\nu\omega_\mu,\\\vec{R}_{\mu\nu}&=\partial_\mu\vec{\rho}_\nu-\partial_\nu\vec{\rho}_\mu-g_\rho(\vec{\rho}_\mu\times\vec{\rho}_\nu),\\F_{\mu\nu}&=\partial_\mu A_\nu-\partial_\nu A_\mu.\end{aligned}\tag{3}$$

The classical variation principle gives equations of motion for the nucleon, mesons, and the photon. As in many applications, we study the ground state properties of nuclei with time reversal symmetry; thus, the nucleon spinors are the eigenvectors of the stationary Dirac equation

$$[\boldsymbol{\alpha}\cdot\boldsymbol{p}+V(\boldsymbol{r})+\beta(M+S(\boldsymbol{r}))]\psi_i(\boldsymbol{r})=\epsilon_i\psi_i(\boldsymbol{r}),\tag{4}$$

and equations of motion for mesons and the photon are

$$\begin{aligned}[-\Delta+\partial_\sigma U(\sigma)]\sigma(\boldsymbol{r})&=-g_\sigma\rho_s(\boldsymbol{r}),\\(-\Delta+m_\omega^2)\omega^0(\boldsymbol{r})&=g_\omega\rho_v(\boldsymbol{r}),\\(-\Delta+m_\rho^2)\rho^0(\boldsymbol{r})&=g_\rho\rho_3(\boldsymbol{r}),\\-\Delta A^0(\boldsymbol{r})&=e\rho_p(\boldsymbol{r}),\end{aligned}\tag{5}$$

where ω^0 and A^0 are timelike components of the vector ω and the photon fields and ρ^0 is the three-component of the timelike component of the isovector vector ρ meson. Equations (4) and (5) are coupled to each other by the vector and scalar potentials

$$\begin{aligned}V(\boldsymbol{r})&=g_\omega\omega^0(\boldsymbol{r})+g_\rho\tau_3\rho^0(\boldsymbol{r})+e\frac{(1-\tau_3)}{2}A^0(\boldsymbol{r}),\\S(\boldsymbol{r})&=g_\sigma\sigma(\boldsymbol{r}),\end{aligned}\tag{6}$$

and various densities

$$\begin{aligned}\rho_s(\boldsymbol{r})&=\sum_{i=1}^{A}\bar{\psi}_i(\boldsymbol{r})\psi_i(\boldsymbol{r}),\\\rho_v(\boldsymbol{r})&=\sum_{i=1}^{A}\psi_i^\dagger(\boldsymbol{r})\psi_i(\boldsymbol{r}),\\\rho_3(\boldsymbol{r})&=\sum_{i=1}^{A}\psi_i^\dagger(\boldsymbol{r})\tau_3\psi_i(\boldsymbol{r}),\end{aligned}$$

$$\rho_c(\boldsymbol{r})=\sum_{i=1}^{A}\psi_i^{\dagger}(\boldsymbol{r})\frac{1-\tau_3}{2}\psi_i(\boldsymbol{r}). \tag{7}$$

For spherical nuclei, meson fields and densities depend only on the radial coordinate r. The spinor is characterized by the angular momentum quantum numbers (l,j), m, the parity, the isospin $t=\pm 1/2$ ("+" for neutrons and "−" for protons), and the radial quantum number α. The Dirac spinor has the form

$$\psi_{\alpha\kappa m}(\boldsymbol{r},s,t)=\begin{pmatrix} i\dfrac{G_\alpha^\kappa(r)}{r}Y_{jm}^{l}(\theta,\phi,s) \\ -\dfrac{F_\alpha^\kappa(r)}{r}Y_{jm}^{\tilde{l}}(\theta,\phi,s)\end{pmatrix}\chi_{t_\alpha}(t), j=l\pm\frac{1}{2}, \tag{8}$$

with $G_\alpha^\kappa(r)/r$ and $F_\alpha^\kappa(r)r$ the radial wave functions for the upper and lower components and $Y_{jm}^{l}(\theta,\phi)$ the spin spherical harmonics where $\kappa=(-1)^{j+l+1/2}(j+1/2)$ and $\tilde{l}=l+(-1)^{j+l-1/2}$. The value of κ from the upper component is used to label a state disregarding that this state is in the Fermi sea or in the Dirac sea. States with the same κ form a "block." The radial equation of the Dirac spinor, Eq. (4), is reduced as

$$\epsilon_\alpha G_\alpha^\kappa=\left(-\frac{\partial}{\partial r}+\frac{\kappa}{r}\right)F_\alpha^\kappa+[M+S(r)+V(r)]G_\alpha^\kappa,$$

$$\epsilon_\alpha F_\alpha^\kappa=\left(+\frac{\partial}{\partial r}+\frac{\kappa}{r}\right)G_\alpha^\kappa-[M+S(r)-V(r)]F_\alpha^\kappa. \tag{9}$$

The meson field equations become simply radial Laplace equations of the form

$$\left(-\frac{\partial^2}{\partial r^2}-\frac{2}{r}\frac{\partial}{\partial r}+m_\phi^2\right)\phi(r)=s_\phi(r). \tag{10}$$

m_ϕ are the meson masses for $\phi=\sigma,\omega,\rho$ and zero for the photon. The source terms are

$$s_\phi(r)=\begin{cases} -g_\sigma\rho_s(r)-g_2\sigma^2(r)-g_3\sigma^3(r) & \text{for } \sigma \\ g_\omega\rho_v(r) & \text{for } \omega \\ g_\rho\rho_3(r) & \text{for } \rho \\ e\rho_c(r) & \text{for } A, \end{cases} \tag{11}$$

with

$$4\pi r^2\rho_s(r)=\sum_{i=1}^{A}(|G_i(r)|^2-|F_i(r)|^2),$$

$$4\pi r^2\rho_v(r)=\sum_{i=1}^{A}(|G_i(r)|^2+|F_i(r)|^2),$$

$$4\pi r^2\rho_3(r)=\sum_{i=1}^{A}2t_i(|G_i(r)|^2+|F_i(r)|^2),$$

$$4\pi r^2\rho_c(r)=\sum_{i=1}^{A}\left(\frac{1}{2}-t_i\right)(|G_i(r)|^2+|F_i(r)|^2). \tag{12}$$

The above coupled equations have been solved in r space [22] and in the HO basis [23] using the no sea and the mean-field approximation. Here we depict briefly the procedure of solving these coupled equations. With a set of estimated meson and photon fields, the scalar and vector potentials are calculated and the radial Dirac equation solved. The so obtained nucleon wave functions are used to calculate the source term of each radial Laplace equation for mesons and the photon. New meson and photon fields are calculated by solving these Laplace equations. This procedure is iterated until a demanded accuracy is achieved. Laplace equations are usually solved by using the Green's function method [22,23] though in Ref. [23] Laplace equations for mesons are solved in the HO basis. SRHR, SRHHO, and SRHWS differ from each other mainly in how the Dirac equation is solved. In the following, the numerical solution of the Dirac equation in the WS basis will be presented.

III. SOLVING THE DIRAC EQUATION IN A WOODS-SAXON BASIS ANDX NUMERICAL DETAILS

A. Woods-Saxon basis from solving a Schrödinger equation (the SWS basis)

For the Schrödinger equation with a spherical Woods-Saxon potential

$$V_{\rm WS}(r)=\begin{cases}\dfrac{V_0}{1+e^{(r-R_0)/a_0}}, & r<R_{\max} \\ \infty, & r\geqslant R_{\max},\end{cases} \tag{13}$$

where $R_{\max}$ is introduced for practical reasons to define the box boundary, the eigenfunction can be written as $\phi_{nlm_l}(\boldsymbol{r})=R_{nl}(r)Y_{lm_l}(\theta,\phi)$. Its radial Schrödinger equation is derived as

$$\left[-\frac{1}{2M}\left(\frac{1}{r^2}\frac{\partial}{\partial r}r^2\frac{\partial}{\partial r}-\frac{l(l+1)}{r^2}\right)+V_{\rm WS}(r)\right]R_{nl}(r) = E_{nl}R_{nl}(r). \tag{14}$$

Equation (14) is solved on a discretized radial mesh with a mesh size Δr. $R_{\max}$ (Δr) should be chosen larger (smaller) enough to make sure that the final results do not depend on it. The radial wave functions thus obtained form a complete basis

$$\{R_{nl}(r);n=0,1,\ldots;l=0,1,\ldots,n\}, \tag{15}$$

in terms of which the radial parts of the upper and the lower components of the Dirac spinor in Eq. (9) are expanded, respectively, as

$$G_\alpha^\kappa(r) = -i\sum_{n=0}^{n_{\max}} g_{\alpha n} r R_{nl}(r),$$

$$F_\alpha^\kappa(r) = -i\sum_{\tilde{n}=0}^{\tilde{n}_{\max}} f_{\alpha\tilde{n}} r R_{\tilde{n}\tilde{l}}(r). \tag{16}$$

The radial Dirac equation, Eq. (9), is transformed into the WS basis as

$$\begin{pmatrix} \mathcal{A}_{mn} & \mathcal{B}_{m\tilde{n}} \\ \mathcal{C}_{\tilde{m}n} & \mathcal{D}_{\tilde{m}\tilde{n}} \end{pmatrix} \begin{pmatrix} g_{\alpha n} \\ f_{\alpha\tilde{n}} \end{pmatrix} = \epsilon_\alpha \begin{pmatrix} g_{\alpha n} \\ f_{\alpha\tilde{n}} \end{pmatrix}, \tag{17}$$

where the matrix elements are calculated as follows

$$\mathcal{A}_{mn} = \int_0^{R_{\max}} r^2 dr R_{ml}(r)(V(r)+S(r)+M)R_{nl}(r),$$

$$\mathcal{B}_{m\tilde{n}} = \int_0^{R_{\max}} r^2 dr R_{ml}(r)\left(+\frac{\partial}{\partial r} - \frac{\kappa_\alpha - 1}{r}\right) R_{\tilde{n}\tilde{l}}(r),$$

$$\mathcal{C}_{\tilde{m}n} = \int_0^{R_{\max}} r^2 dr R_{\tilde{m}\tilde{l}}(r)\left(-\frac{\partial}{\partial r} - \frac{\kappa_\alpha + 1}{r}\right) R_{nl}(r),$$

$$\mathcal{D}_{\tilde{m}\tilde{n}} = \int_0^{R_{\max}} r^2 dr R_{\tilde{m}\tilde{l}}(r)(V(r)-S(r)-M)R_{\tilde{n}\tilde{l}}(r). \tag{18}$$

In practical calculations, an energy cutoff $E_{\rm cut}$ (relative to the nucleon mass M) is used to determine the cutoff of the radial quantum number $n_{\max}$ for each block. In the expansion of the corresponding lower component, we take $\tilde{n}_{\max} = n_{\max} + \Delta n$ with $\Delta n \geqslant 1$ in order to avoid spurious states [23].

The following Woods-Saxon parameters have been used according to Ref. [25]:

$$V_0 = [-51 \pm 33(N-Z)/A] \text{ MeV},$$

$$R_0 = 1.27A^{1/3} \text{ fm}, \quad a_0 = 0.67 \text{ fm}, \tag{19}$$

where "+" is for the neutron and "−" for the proton. As expected, the dependence of final results on the initial WS potential is almost negligible. For example, a variation of V_0 by 50% gives a difference in total binding energies by less than 0.1% and a difference in charge radii by less than 0.5% for ^{16}O, ^{48}Ca, and ^{208}Pb. Such a situation is also checked to be true for the other two parameters in the WS potential, R_0 and a_0.

B. Woods-Saxon basis from solving a Dirac equation (the DWS basis)

The radial Dirac equation, Eq. (9), may be solved in r space [22] with Woods-Saxon-like potentials for $V_0(r) \pm S_0(r)$ [24] within a spherical box of size $R_{\max}$, together with the spherical spinor which gives a complete WS basis

$$\{[\epsilon^0_{n\kappa m}, \psi^0_{n\kappa m}(\boldsymbol{r},s,t)]; \epsilon^0_{n\kappa m} \gtrless 0\}, \tag{20}$$

with $n = 0,1,\ldots,$ $\kappa = \pm 1, \pm 2, \ldots,$ and $m = -j_\kappa, \ldots, j_\kappa$. $\psi^0_{n\kappa m}(\boldsymbol{r},s,t)$ takes the form of Eq. (8). We note that states both in the Fermi sea and in the Dirac sea should be included in the basis for completeness. The nucleon wave function, Eq. (8), can be expanded in terms of this set of basis as

$$\psi_{\alpha\kappa m}(\boldsymbol{r},s,t) = \sum_{n=0}^{n_{\max}} c_{\alpha n} \psi^0_{n\kappa m}(\boldsymbol{r},s,t), \tag{21}$$

where $n_{\max} = n^+_{\max} + n^-_{\max} + 1$ and the summation is over positive energy levels in the Fermi sea for $0 \leqslant n \leqslant n^+_{\max}$ and over negative energy levels in the Dirac sea for $n^+_{\max}+1 \leqslant n \leqslant n_{\max}$. The negative energy states are obtained with the same method as the positive energy ones [22]. In this WS basis, the Dirac equation, Eq. (4), turns out to be

$$c_{\alpha m}\epsilon^0_m + \sum_{n=0}^{n_{\max}} c_{\alpha n} H'_{mn} = \epsilon_\alpha c_{\alpha m}, m = 1, \ldots, n_{\max}, \tag{22}$$

with

$$\begin{aligned} H'_{mn} &= \langle \psi^0_m(\boldsymbol{r}) | [\Delta V(\boldsymbol{r}) + \beta \Delta S(\boldsymbol{r})] | \psi^0_n(\boldsymbol{r}) \rangle \\ &= \int_0^{R_{\max}} dr G^0_m(r)[\Delta V(r) + \Delta S(r)] G^0_n(r) \\ &\quad + \int_0^{R_{\max}} dr F^0_m(r)[\Delta V(r) - \Delta S(r)] F^0_n(r), \end{aligned} \tag{23}$$

where $\Delta V(\boldsymbol{r}) = V(\boldsymbol{r}) - V_0(\boldsymbol{r})$ and $\Delta S(\boldsymbol{r}) = S(\boldsymbol{r}) - S_0(\boldsymbol{r})$. The angular, spin, and isospin quantum numbers are omitted for brevity.

It should be mentioned that Eq. (9) can be solved directly in r space with the same method of generating the DWS basis. It is our aim to test the validity of an efficient solution not only for the spherical RH model but also for its extension to include the deformation and/or pairing correlations. In fact, if only the SRH theory is concerned, this procedure is just a replacement of the direct solution in r space by a diagonalization of a matrix with some complication introduced by the fact that contributions from states in the Dirac sea must be included.

An energy cutoff $E_{\rm cut}$ (relative to the nucleon mass M) and the cutoff of radial quantum numbers $n^+_{\max}$ are applied to positive energy levels alternatively according to practical convenience. For the initial Woods-Saxon potentials $V_0(r) \pm S_0(r)$, we follow Ref. [24].

C. Comparison with the r-space method

In order to check the validity of solving the Dirac equation in the WS basis and to provide numerical experiences for future applications, we compare the results of ^{16}O and ^{208}Pb obtained from solving the Dirac equation in the WS basis and those from solving the same equation in the coordinate space. The latter is the most accurate method of solving the Dirac equation for realistic nuclei up to now and thus is used as a standard here. The scalar and vector potentials in the Dirac equation are provided by very accurate SRHR cal-

TABLE I. Dependence of the average single-particle energy, root mean square (rms) radius, and $\langle r^4\rangle^{1/4}$ on the mesh size Δr for the SRHSWS theory. The meson and Coulomb fields are obtained from SRHR calculations with the parameter set NL3, $\Delta r=0.05$ fm, and $R_{max}=30$ fm for ^{16}O and 35 fm for ^{208}Pb. In SRHSWS calculations, the parameter set NL3 is used. For ^{16}O, $R_{max}=4r_0A^{1/3}=12.8$ fm and $E_{cut}=300$ MeV. For ^{208}Pb, $R_{max}=3r_0A^{1/3}=22.6$ fm and $E_{cut}=200$ MeV. The first row gives results from solving the Dirac equation in the coordinate space.

Δr	$-E_{sp}/A$	$\langle r^2\rangle^{1/2}$	$\langle r^4\rangle^{1/4}$	$-E_{sp}/A$	$\langle r^2\rangle^{1/2}$	$\langle r^4\rangle^{1/4}$
		^{16}O			^{208}Pb	
	23.0375	2.5945	2.8900	23.3348	5.6315	5.9883
0.05	23.0375	2.5945	2.8900	23.3348	5.6315	5.9883
0.10	23.0376	2.5945	2.8899	23.3348	5.6315	5.9883
0.20	23.0385	2.5941	2.8896	23.3347	5.6315	5.9883
0.30	23.0430	2.5930	2.8889	23.3343	5.6314	5.9883
0.40	23.0420	2.5923	2.8885	23.3334	5.6315	5.9885
0.50	22.9887	2.5949	2.8936	23.3284	5.6319	5.9890

culations with the parameter set NL3 for the Lagrangian, the mesh size $\Delta r=0.05$ fm, and the box size $R_{max}=30$ fm for ^{16}O and $R_{max}=35$ fm for ^{208}Pb. Then with $S(r)$ and $V(r)$ thus obtained, the Dirac equation is solved in the coordinate space and in the WS basis with the parameter set NL3 also.

To compare the results obtained only from solving the Dirac equation avoids errors from other numerical procedures, e.g., the error from the iteration and that from solving the Laplace equations. For the same reason, what we compare between these two methods is not the binding energy, which contains the contribution from mesons, but the average single-particle energy E^{sp}/A; $E^{sp}=\Sigma_i\epsilon_i$, where ϵ_i is the single-particle energy and the summation runs over all occupied states for both neutrons and protons. We also compare the rms radii $\langle r^2\rangle^{1/2}$ and $\langle r^4\rangle^{1/4}$. The radius $\langle r^4\rangle^{1/4}$ reflects the nucleon densities in the large r region more than the rms radius does.

Table I presents the dependence of results of the Dirac equation in the SWS basis on the mesh size Δr. With Δr decreasing, results in the SWS basis approach the standard results, i.e., those in r space. $\Delta r=0.1$ fm gives results accurately enough. The dependence on the box size R_{max} and on the basis size determined by E_{cut} are investigated and shown in Figs. 1 and 2 where the deviations of the average single particle energy E^{sp}/A, the rms radii $\langle r^2\rangle^{1/2}$ and $\langle r^4\rangle^{1/4}$ from the standards are plotted versus E_{cut}, for different R_{max}. If R_{max} is not large enough, it is difficult to approach the standard results. For example, when $R_{max}=3r_0A^{1/3}=9.4$ fm and $E_{cut}=300$ MeV for ^{16}O (correspondingly, $N_{max}\sim 20$), the results seem converged, but the discrepancy of the average single-particle energy from the standard one remains 0.1 keV (Table II). So one must use a large enough box with a size R_{max} around $4r_0A^{1/3}$ for light nuclei and $3r_0A^{1/3}$ for heavy ones. It is interesting that the convergence of the results does not depend on N_{max}, but only on E_{cut}. For ^{16}O (^{208}Pb), the results converge to the standard ones at $\sim$ 300 (400) MeV. From Figs. 1 and 2, we find that the radius $\langle r^4\rangle^{1/4}$ also converges very well, which implies that nucleon densities can be calculated accurately even for large r.

We have made similar investigations for results in the DWS basis and the same conclusions are drawn. For instance, the deviations of the average single-particle energy E^{sp}/A, the rms radii $\langle r^2\rangle^{1/2}$ and $\langle r^4\rangle^{1/4}$ from the standards are plotted versus E_{cut} for different R_{max} in Figs. 3 and 4.

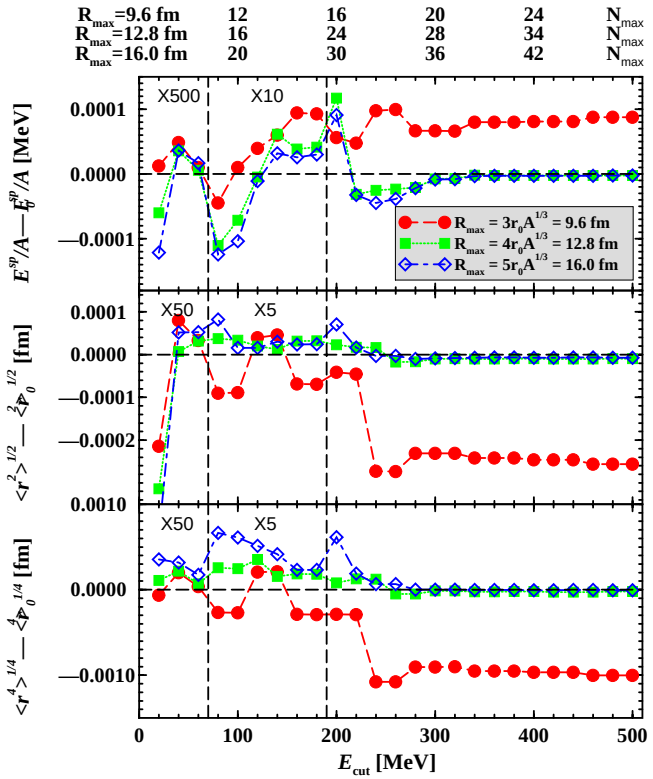

FIG. 1. (Color online) Deviations of the average single-particle energy E^{sp}/A (the upper panel), rms radius $\langle r\rangle^{1/2}$ (the middle panel), and $\langle r^4\rangle^{1/4}$ (the lower panel) of ^{16}O from the standard results versus the cutoff energy E_{cut} with a different box size R_{max} for the SRHSWS theory. The meson and Coulomb fields are obtained from SRHR calculations with the parameter set NL3, $\Delta r=0.05$ fm, and $R_{max}=30$ fm. In SRHSWS calculations, the parameter set NL3 is used. For $E_{cut}=100$, 200, 300, and 400 MeV, the approximate maximum principal quantum number in each basis, $N_{max}=2n_{max}+l$, is given on the top of the plot.

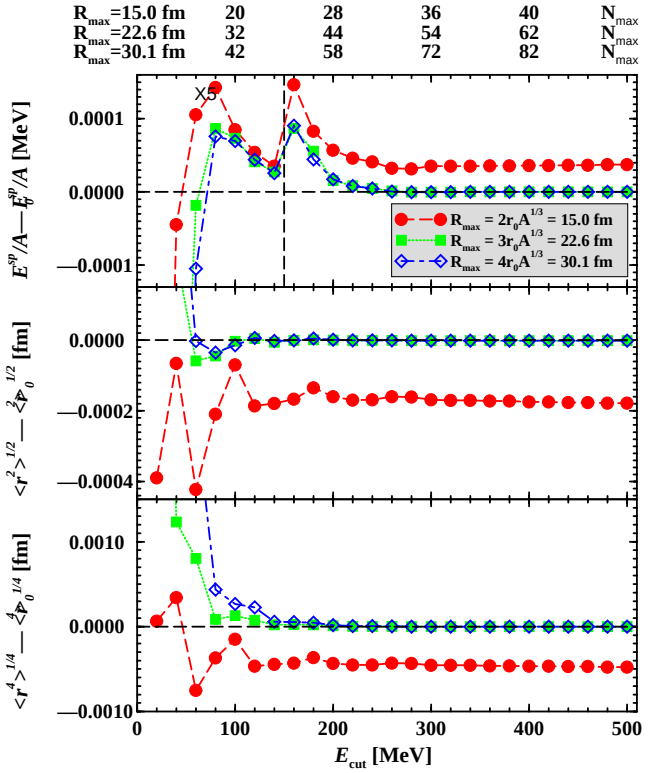

FIG. 2. (Color online) Deviations of the average single-particle energy E^{sp}/A (the upper panel), rms radius $\langle r\rangle^{1/2}$ (the middle panel), and $\langle r^4\rangle^{1/4}$ (the lower panel) of ^{208}Pb from the standard results versus the cutoff energy E_{cut} with a different box size $R_{\max}$ for the SRHSWS theory. The meson and Coulomb fields are obtained from SRHR calculations with the parameter set NL3, $\Delta r=0.05$ fm, $R_{\max}=35$ fm. In SRHSWS calculations, the parameter set NL3 is used. For $E_{\mathrm{cut}}=100$, 200, 300, and 400 MeV, the approximate maximum principal quantum number in each basis, $N_{\max}=2n_{\max}+l$, is given on the top of the plot.

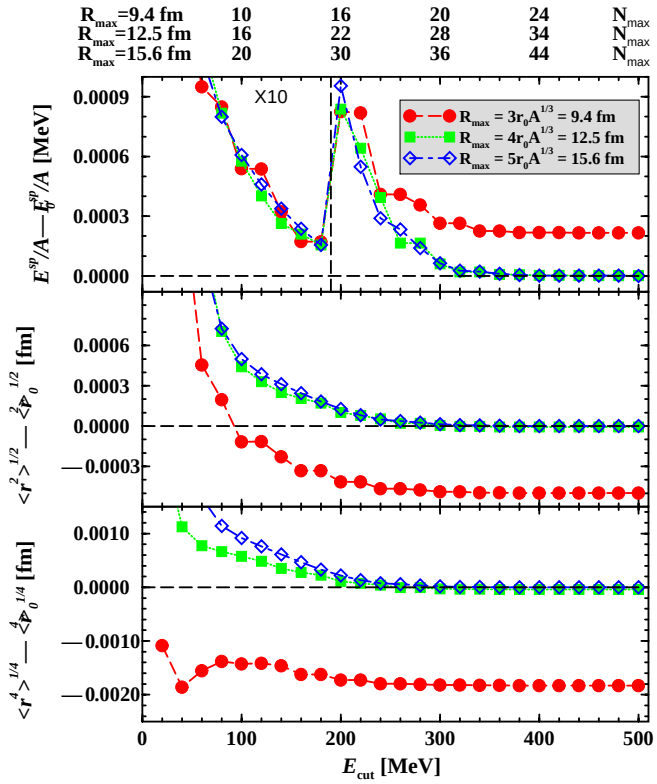

FIG. 3. (Color online) Deviations of the average single-particle energy E^{sp}/A (the upper panel), rms radius $\langle r\rangle^{1/2}$ (the middle panel), and $\langle r^4\rangle^{1/4}$ (the lower panel) of ^{16}O from the standard results versus the cutoff energy E_{cut} with a different box size $R_{\max}$ for the SRHDWS theory. The meson and Coulomb fields are obtained from SRHR calculations with the parameter set NL3, $\Delta r=0.05$ fm and $R_{\max}=30$ fm. In SRHDWS calculations, the parameter set NL3 is used. For $E_{\mathrm{cut}}=100$, 200, 300, and 400 MeV, the approximate maximum principal quantum number in each basis, $N_{\max}=2n_{\max}+l$, is given on the top of the plot.

TABLE II. Dependence of the average single-particle energy, rms radius, and $\langle r^4\rangle^{1/4}$ on the difference $\Delta n=\tilde{n}_{\max}-n_{\max}$ for the SRHSWS theory. The meson and Coulomb fields are obtained from SRHR calculations with the parameter set NL3, $\Delta r=0.05$ fm, and $R_{\max}=30$ fm for ^{16}O and 35 fm for ^{208}Pb. In SRHSWS calculations, the parameter set NL3 is used. For ^{16}O, $R_{\max}=4r_0A^{1/3}=12.8$ fm. For ^{208}Pb, $R_{\max}=3r_0A^{1/3}=22.6$ fm.

Δn	$-E_{\mathrm{sp}}/A$	$\langle r^2\rangle^{1/2}$	$\langle r^4\rangle^{1/4}$	$-E_{\mathrm{sp}}/A$	$\langle r^2\rangle^{1/2}$	$\langle r^4\rangle^{1/4}$
	^{16}O: $E_{\mathrm{cut}}=100$ MeV			^{208}Pb: $E_{\mathrm{cut}}=100$ MeV		
1	23.0382	2.5947	2.8920	23.3344	5.6315	5.9884
3	23.0326	2.5949	2.8913	23.3341	5.6315	5.9884
5	23.0298	2.5952	2.8915	23.3340	5.6315	5.9884
7	23.0290	2.5953	2.8915	23.3340	5.6315	5.9884
9	23.0289	2.5953	2.8915	23.3340	5.6315	5.9884
	^{16}O: $E_{\mathrm{cut}}=300$ MeV			^{208}Pb: $E_{\mathrm{cut}}=200$ MeV		
1	23.0375	2.5945	2.8999	23.3348	5.6315	5.9883
3	23.0375	2.5945	2.8999	23.3348	5.6315	5.9883
5	23.0375	2.5945	2.8999	23.3347	5.6315	5.9883
7	23.0375	2.5945	2.8999	23.3347	5.6315	5.9883
9	23.0375	2.5945	2.8999	23.3347	5.6315	5.9883

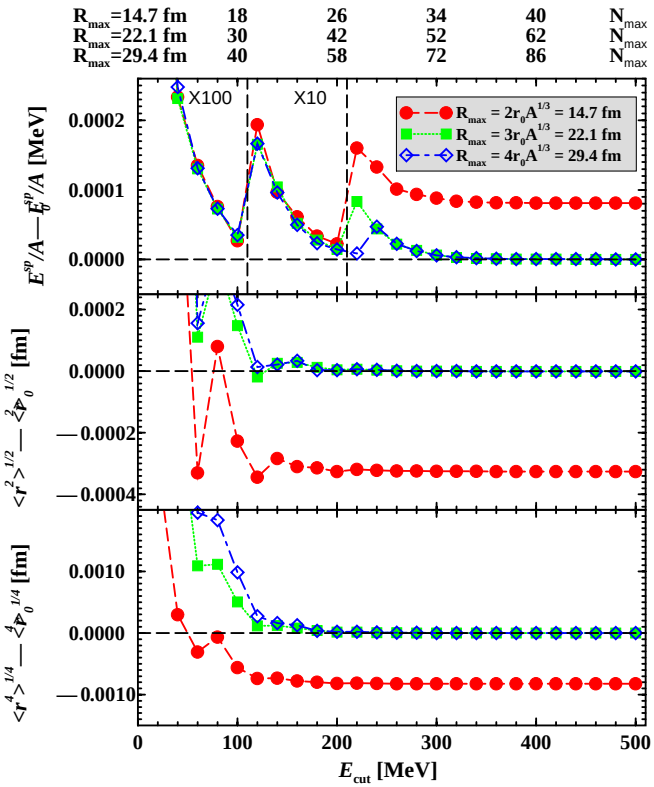

FIG. 4. (Color online) Deviations of the average single-particle energy E^{sp}/A (the upper panel), rms radius $\langle r\rangle^{1/2}$ (the middle panel), and $\langle r^4\rangle^{1/4}$ (the lower panel) of ^{208}Pb from the standard results versus the cutoff energy E_{cut} with a different box size R_{max} for the SRHDWS theory. The meson and Coulomb fields are obtained from SRHR calculations with the parameter set NL3, $\Delta r = 0.05$ fm, and $R_{\mathrm{max}}=35$ fm. In SRHDWS calculations, the parameter set NL3 is used. For $E_{\mathrm{cut}}=100$, 200, 300, and 400 MeV, the approximate maximum principal quantum number in each basis, $N_{\mathrm{max}}=2n_{\mathrm{max}}+l$, is given on the top of the plot.

In the expansion of the nucleon wave function, Eq. (21), one has to take into account not only the levels in the Fermi sea but also those in the Dirac sea because together they form a complete basis. Now the question arises of how many levels in the Dirac sea one has to take into account. In the calculations in Figs. 3 and 4, we have used $n^-_{\mathrm{max}}=n^+_{\mathrm{max}}$ with n^+_{max} determined by E_{cut}. In Table III, the dependence of the average single-particle energy, the rms radii $\langle r^2\rangle^{1/2}$ and $\langle r^4\rangle^{1/4}$ on $N^-_{\mathrm{max}}=2n^-_{\mathrm{max}}+l$—a cutoff on the principal quantum number of levels in the Dirac sea—are given for ^{16}O and ^{208}Pb. From Table III, we find the merit of solving the Dirac equation in the DWS basis: the number of negative energy states included in the basis could be much smaller than that of the positive energy states. Let us take ^{16}O as an example, $R_{\mathrm{max}}=4r_0A^{1/3}$ and $E_{\mathrm{cut}}=300$ MeV for positive energy states correspond to $N^+_{\mathrm{max}}\sim 28$. For negative energy states, $N^-_{\mathrm{max}}=10$ gives very accurate results, e.g., the discrepancy of E^{sp}/A from the standard is smaller than 0.1 keV. This will significantly simplify the deformed problem by decreasing the matrix dimension compared to the solution of the Dirac equation in the SWS basis.

The above investigations are somehow academic. In practical applications, it is not necessary to go to an accuracy of some keV in the single-particle energy or 10^{-4} fm in the radius. So in the following calculations, we will use $R_{\mathrm{max}}=20$ fm, $\Delta r=0.1$ fm, and $E_{\mathrm{cut}}=60$–80 MeV for heavy and light nuclei, which give reasonable accuracies both for the binding energy and the radius. This set of cutoffs corresponds approximately to $N_{\mathrm{max}}=2n_{\mathrm{max}}+l\sim 25$, where l is the orbital angular momentum of relevant state.

IV. RESULTS AND DISCUSSION

In this section, we present results of SRHWS. Since our main aim is to show the virtues of SRHWS compared to SRHHO and SRHR, we do not include pairing correlations and restrict our study to doubly magic or magic nuclei only. If not specified, the parameter set NLSH is used for the Lagrangian, $R_{\mathrm{max}}=20$ fm, and $\Delta r=0.1$ fm throughout this section. Other parameter sets for the Lagrangian do not change the conclusion here. In SRHDWS, the number of positive energy levels in the Fermi sea and that of negative energy ones in the Dirac sea are the same for convenience, i.e., $n^+_{\mathrm{max}}=n^-_{\mathrm{max}}$. For SRHHO, $\hbar\omega_0=41A^{-1/3}$ has been used and cutoffs of the expansion for fermions and bosons are the same, i.e., $N_{\mathrm{F}}=N_{\mathrm{B}}\equiv N_{\mathrm{max}}$.

A. Bulk properties of stable nuclei from different SRH theories

In Table IV, the binding energy per nucleon (E/A), and neutron, proton, and charge radii (r_{n}, r_{p}, and r_{c}) of some typical spherical nuclei are presented, which are calculated from the present available codes, including SRHR, SRHSWS, SRHDWS, and SRHHO. Available data [26,27] are also included for comparison. We use approximately the same N_{max} in the SRHHO as that in the SRHWS which is determined by E_{cut}.

Generally speaking, for each studied nucleus, the four approaches give almost the same results with an accuracy within 0.1% with few exceptions where the differences are still less than 0.3%. They are in excellent agreement with available data.

With the same parameters of spatial lattice, R_{max} and Δr, SRHWS should reproduce results of SRHR when E_{cut} (or N_{max}) is large enough. This is justified in Table IV. One can find exactly coincident results between SRHSWS and SRHR for most of the studied nuclei. The remaining differences and those between SRHDWS and SRHR could be diminished by increasing E_{cut}.

In Fig. 5, the neutron density distributions are compared between SRHR, SRHSWS, SRHDWS, and SRHHO, in which ^{16}O is chosen as an example. Comparisons are also made for heavier nuclei such as ^{48}Ca and ^{208}Pb. Similar results are obtained and not shown here. The calculation details are the same as Table IV. For these stable nuclei, all of these SRH methods are valid and all calculations are in excellent agreement with each other from the central to the outer region of each nucleus. Small differences in the central region do not affect the physical observables, such as the

TABLE III. Dependence of the single particle energy, rms radius, and $\langle r^4\rangle^{1/4}$ on the maximum principal quantum number $N^-_{\max}=2n^-_{\max}+l$ for the SRHDWS theory. The meson and Coulomb fields are obtained from SRHR calculations with the parameter set NL3, $\Delta r=0.05$ fm, and $R_{\max}=30$ fm for ^{16}O and 35 fm for ^{208}Pb. In SRHDWS calculations, the parameter set NL3 is used. For ^{16}O, $R_{\max}=4r_0A^{1/3}=12.5$ fm and $E_{\rm cut}=300$ MeV for positive energy states. For ^{208}Pb, $R_{\max}=3r_0A^{1/3}=22.1$ fm and $E_{\rm cut}=200$ MeV for positive energy states.

$\widetilde{N}_{\max}$	$-E_{\rm sp}/A$	$\langle r^2\rangle^{1/2}$	$\langle r^4\rangle^{1/4}$	$-E_{\rm sp}/A$	$\langle r^2\rangle^{1/2}$	$\langle r^4\rangle^{1/4}$
		^{16}O			^{208}Pb	
no	23.1129	2.5912	2.8859	23.3331	5.6314	5.9889
0	23.1077	2.5916	2.8861	23.3329	5.6314	5.9889
2	23.0762	2.5939	2.8889	23.3316	5.6315	5.9890
4	23.0617	2.5942	2.8893	23.3304	5.6317	5.9892
6	23.0439	2.5946	2.8898	23.3299	5.6318	5.9893
8	23.0385	2.5946	2.8899	23.3294	5.6319	5.9893
10	23.0376	2.5946	2.8899	23.3292	5.6319	5.9894
12	23.0375	2.5946	2.8899	23.3291	5.6319	5.9899
14	23.0375	2.5946	2.8899	23.3290	5.6319	5.9894
16	23.0375	2.5946	2.8899	23.3290	5.6319	5.9894
18	23.0375	2.5946	2.8899	23.3289	5.6319	5.9893
20	23.0375	2.5946	2.8899	23.3288	5.6319	5.9893
22	23.0375	2.5946	2.8899	23.3287	5.6319	5.9893
30	23.0375	2.5946	2.8899	23.3287	5.6319	5.9893

binding energy or nuclear radius, as is seen in Table IV. Furthermore, these differences could also be decreased by increasing $E_{\rm cut}$ or $N_{\max}$.

From the above discussions, it is clear that SRHWS is equivalent to SRHR and SRHHO for stable nuclei. Thus, we conclude that the Woods-Saxon basis provides another possibility to solve the (non-)relativistic mean-field theory.

B. Neutron density distributions for ^{72}Ca in different SRH theories

As already discussed in the Introduction, one of the merits of SRHR against SRHHO is its proper description of exotic nuclei. In this section, we will demonstrate the equivalence between SRHWS and SRHR when reasonably large $E_{\rm cut}$ is applied in SRHWS.

In order to see the results for the unstable nuclei near the neutron drip line, the neutron density distribution for ^{72}Ca is studied here. The nucleus ^{72}Ca is predicted to be the last bound calcium isotope [28–31]. Since it is not a doubly magic nucleus, there might be some uncertainty in the present results due to the lack of inclusion of pairing correlations. However, as stressed in the beginning of this section, the main aim here is to show the equivalence between SRHWS and SRHR, it is very unlikely that pairing correlations would change our conclusion qualitatively.

For stable nuclei, it has been shown that $R_{\max}\sim 20$ fm is large enough. For drip line nuclei, the dependence of the results on $R_{\max}$ for ^{72}Ca is presented in Table V. For both SRHR and SRHWS, $\Delta r=0.1$ fm and $R_{\max}=20$, 25, 30, and 35 fm have been used, respectively. The energy cutoff $E_{\rm cut}=75$ MeV is used in SRHWS calculations. In SRHR and SRHWS calculations, the neutron rms radius $r_{\rm n}$ and the Fermi energy $\lambda_{\rm n}$ of ^{72}Ca converge around $R_{\max}=35$ fm. The binding energy per nucleon E/A and the proton rms radius $r_{\rm p}$ are almost independent of the box size when $R_{\max}$ is larger than 20 fm. $E_{\rm cut}=75$ MeV and $R_{\max}=20$, 25, 30, and 35 fm in SRHWS correspond to cutoffs on the principal quantum number $N_{\max}=25$, 31, 37, and 43, which are used in SRHHO calculations in order to make fair comparisons between SRHWS and SRHHO. Similar to those from SRHR and SRHWS, E/A and $r_{\rm p}$ depend little on $N_{\max}$ in SRHHO. However, the neutron rms radius $r_{\rm n}$ increases steadily with $N_{\max}$, which shows a much slower convergence. As it is based on a complete basis, SRHHO can also reach convergence of $r_{\rm n}$ if $N_{\max}$ is large enough. From Table V, one finds that for the same $N_{\max}$ (or equivalent $R_{\max}$), a difference of $\Delta r_{\rm n}\approx 0.2$ fm between SRHHO and SRHWS (SRHR) can be seen. From the slow convergence of $r_{\rm n}$ with $N_{\max}$ in SRHHO ($\Delta N_{\max}=6$ gives $\Delta r_{\rm n}\approx 0.02$ fm), we can estimate the lower limit of $N_{\max}$ as $N_{\max}\approx 90$ in order to give $r_{\rm n}=4.8$ fm.

We compare the neutron density distribution of ^{72}Ca from different SRH approaches in Fig. 6. With the same box size, the density distribution from SRHR are almost identical with those from SRHWS, which indicates the equivalence between SRHWS and SRHR. For brevity, only $\rho_{\rm n}(r)$ from SRHR with $R_{\max}=35$ fm is displayed in Fig. 6 which covers the curve corresponding to $\rho_n(r)$ from SRHWS with $R_{\max}=35$ fm in Fig. 6. On the other hand, $\rho_{\rm n}(r)$ from SRHHO even with $N_{\max}=43$ fails to reproduce the result of SRHR due to the well known localization property of the HO potential [9].

This result is very encouraging and shows us that even the long tail (or halo) behavior in neutron density distribution for nuclei near the drip line can be described by SRHSWS as well as SRHR, if pairing correlations are incorporated properly.

TABLE IV. The binding energy per nucleon, and neutron, proton and charge radii of some typically spherical nuclei. The parameter set NLSH is used for the Lagrangian. $R_{max}=20$ fm and $\Delta r=0.1$ fm for SRHR and SRHWS. $\hbar\omega_0=41A^{-1/3}$ for SRHHO. Numbers in brackets in the second column give E_{cut} for SRHWS and N_{max} for SRHHO. Data for E/A and r_c are taken from Refs. [26] and [27], respectively. Energy is in MeV and radius in fm.

Nucleus		E/A	r_n	r_p	r_c
^{16}O	SRHR	−8.022	2.551	2.578	2.699
	SRHSWS (80)	−8.022	2.554	2.581	2.702
	SRHDWS (80)	−8.014	2.553	2.580	2.701
	SRHHO (25)	−8.034	2.551	2.577	2.699
	Experiment	−7.976			2.693
^{40}Ca	SRHR	−8.500	3.311	3.359	3.452
	SRHSWS (80)	−8.499	3.310	3.358	3.452
	SRHDWS (80)	−8.497	3.312	3.359	3.453
	SRHHO (25)	−8.514	3.310	3.358	3.452
	Experiment	−8.551			3.478
^{48}Ca	SRHR	−8.644	3.586	3.369	3.463
	SRHSWS (80)	−8.646	3.583	3.368	3.461
	SRHDWS (80)	−8.639	3.586	3.371	3.464
	SRHHO (25)	−8.659	3.584	3.368	3.462
	Experiment	−8.666			3.479
^{56}Ni	SRHR	−8.634	3.582	3.630	3.717
	SRHSWS (80)	−8.640	3.580	3.628	3.715
	SRHDWS (80)	−8.625	3.585	2.633	3.720
	SRHHO (25)	−8.650	3.581	3.629	3.716
	Experiment	−8.345			
^{90}Zr	SRHR	−8.677	4.294	4.186	4.262
	SRHSWS (75)	−8.677	4.295	4.187	4.263
	SRHDWS (75)	−8.672	4.295	4.187	4.262
	SRHHO (25)	−8.693	4.293	4.185	4.261
	Experiment	−8.710			4.270
^{118}Sn	SRHR	−8.466	4.743	4.553	4.623
	SRHSWS (70)	−8.466	4.743	4.554	4.624
	SRHDWS (70)	−8.460	4.743	4.554	4.624
	SRHHO (25)	−8.482	4.741	4.552	4.622
	Experiment	−8.517			4.641
^{132}Sn	SRHR	−8.377	4.964	4.636	4.704
	SRHSWS (70)	−8.377	4.964	4.637	4.704
	SRHDWS (70)	−8.370	4.964	4.637	4.706
	SRHHO (25)	−8.393	4.963	4.635	4.703
	Experiment	−8.355			
^{208}Pb	SRHR	−7.885	5.713	5.447	5.505
	SRHSWS (60)	−7.886	5.712	5.447	5.505
	SRHDWS (60)	−7.874	5.712	5.448	5.506
	SRHHO (25)	−7.900	5.711	5.445	5.504
	Experiment	−7.868			5.504

C. Contribution from negative energy levels in the SRHDWS theory

In the expansion of the nucleon wave function, Eq. (21), one has to take into account not only the states in the Fermi sea but also those in the Dirac sea because these states form a complete basis together. We study the contribution from negative energy states for ^{16}O. The results are given in Table VI. First, without negative energy levels included, the nucleus is overbound and the nuclear size is smaller as seen from Table VI. Second, contrary to the case with negative energy levels included, the calculated nuclear properties depend on the initial potentials very much if no negative energy levels are included.

It should be noted that the contribution from negative energy levels depends on the initial Woods-Saxon potentials for generating the DWS basis. So do the cutoff N_{max} or E_{cut} for convergence. If the initial Woods-Saxon potential is exactly identical to the converged potentials, the matrix in Eq. (22) is

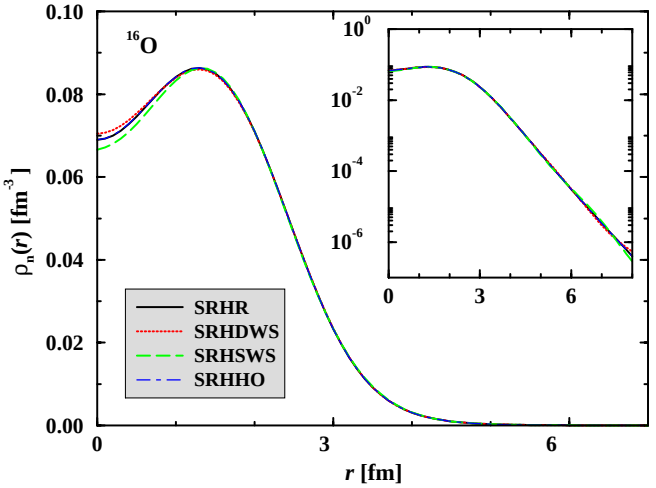

FIG. 5. (Color online) Neutron density distributions for ^{16}O from different SRH approaches. The parameter set NLSH is used for the Lagrangian. $R_{max}=20$ fm and $\Delta r=0.1$ fm for SRHR and SRHWS. $E_{cut}=80$ MeV for SRHWS. Correspondingly, $N_{max}=25$ for SRHHO. In SRHDWS, the number of levels in the Dirac sea included in each block is the same as that of levels in the Fermi sea which is determined by E_{cut}. The inset presents logarithmic densities.

diagonal, negative energy states do not contribute because of the no sea approximation. Positive energy states can also be chosen as less as possible, e.g., $1s_{1/2}$, $1p_{3/2}$, and $1p_{1/2}$ are enough for ^{16}O. From the third column corresponding to

TABLE V. Convergence study for ^{72}Ca. The parameter set NLSH is used for the Lagrangian. $\Delta r=0.1$ fm for SRHR and SRHWS. $E_{cut}=75$ MeV for SRHWS. Energy is in MeV and radius in fm.

	E/A	r_n	r_p	λ_n
R_{max}		SRHR		
20	6.482	4.656	3.639	−0.191
25	6.483	4.723	3.639	−0.221
30	6.484	4.773	3.639	−0.228
35	6.484	4.807	3.639	−0.229
R_{max}		SRHSWS		
20	6.481	4.663	3.639	−0.206
25	6.482	4.726	3.639	−0.231
30	6.483	4.774	3.639	−0.237
35	6.483	4.803	3.639	−0.238
R_{max}		SRHDWS		
20	6.474	4.662	3.641	−0.163
25	6.475	4.733	3.641	−0.197
30	6.475	4.789	3.640	−0.205
35	6.475	4.828	3.640	−0.206
N_{max}		SRHHO		
25	6.489	4.577	3.639	−0.054
31	6.492	4.605	3.639	−0.128
37	6.494	4.628	3.639	−0.166
43	6.494	4.649	3.639	−0.189

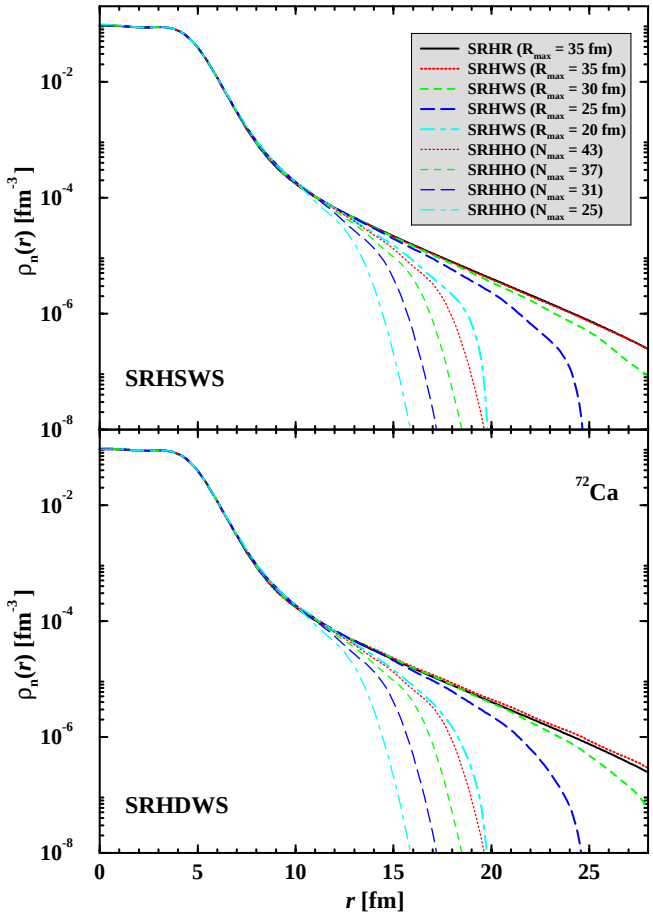

FIG. 6. (Color online) Comparison of density distributions for ^{72}Ca from SRHR, SRHWS, and SRHHO. The parameter set NLSH is used for the Lagrangian. $\Delta r=0.1$ fm for SRHR and SRHWS. $E_{cut}=75$ MeV and $R_{max}=20$ (thick dot-dashed curve), 25 (thick long-dashed curve), 30 (thick dashed curve), and 35 fm (thick dotted curve) for SRHWS. Note that the legend is for both SRHSWS (the upper panel) and SRHDWS (the lower panel). These sets of cutoffs correspond to cutoffs in principal quantum number $N_{max}=25$ (thin dot-dashed curve), 31 (thin long-dashed curve), 37 (thin dashed curve), and 43 (thin dotted curve) which are used in SRHHO calculations. The density distribution from SRHR are almost identical with that from SRHWS with the same box size. For brevity, only $\rho_n(r)$ from SRHR with $R_{max}=35$ fm (thick solid line) is displayed here.

$V_0=72$ MeV in Table VI, one finds that the initial nuclear potential for the Dirac equation proposed in Ref. [24] is a good choice for SRHDWS as the negative energy states only contribute $\sim$1.25% to both E/A and r_{rms}. If we change the initial potentials, e.g., by changing V_0 by 25%, much larger contributions from negative energy states are found in Table VI.

In order to know the contribution of negative energy states in the Dirac sea to the wave function, the value of $\Sigma_n|c_n^-|^2$ in the expansion, Eq. (21) has been calculated for occupied states of ^{16}O. We found a small contribution, the value of $\Sigma_n|c_n^-|^2$ is around 10^{-4} to 10^-5. Note that the nucleon wave function is normalized to one. However, such

TABLE VI. Effects of negative energy levels on bulk properties in SRHDWS for ^{16}O. The parameter set for the Lagrangian is NLSH, $R_{max}=20$ fm, $\Delta r=0.1$ fm, and $N^{+}_{max}=25$. For the initial Woods-Saxon-like potentials, parameters in Ref. [24] are used except for V_0 which is specified in the table. The left value in each entry gives the result without negative energy levels included and the right one that with $N^{-}_{max}=25$. Energy is in MeV and radius in fm.

	$V_0=54$ MeV	$V_0=72$ MeV	$V_0=90$ MeV
E/A	8.547 | 8.013	8.117 | 8.015	8.427 | 8.012
r_{rms}	2.385 | 2.568	2.531 | 2.567	2.610 | 2.567

a small component from negative energy states in the wave functions contributes to the physical observables, such as E/A and r_{rms}, by magnitudes of 1–10% as seen from Table VI. Again, we note that the initial Woods-Saxon potentials differ more from the converged ones, the larger the contribution from negative energy levels.

V. SUMMARY

We have solved the spherical relativistic Hartree theory in the Woods-Saxon basis (SRHWS). The Woods-Saxon basis is obtained by solving either the Schrödinger equation (SRHSWS) or the Dirac equation (SRHDWS). Formalism and numerical details for both cases are presented. The WS basis in the SRHDWS theory could be much smaller than that in the SRHSWS theory. This will largely facilitate the deformed problem.

The results from SRHWS are compared with those from solving the spherical relativistic Hartree theory in the harmonic oscillator basis, SRHHO, and those in the coordinate space, SRHR. For stable nuclei, all approaches give identical results for properties such as total binding energies, the neutron, proton, and charge rms radii, as well as neutron density distributions.

For neutron drip line nuclei, e.g., ^{72}Ca, which has a very small neutron Fermi energy $\lambda_n \sim 0.2$ MeV, both SRHR and SRHWS easily approach convergence by increasing box size, while SRHHO does not. Furthermore, SRHWS can satisfactorily reproduce the neutron density distribution from SRHR, but SRHHO fails with similar cutoffs.

In SRHDWS calculations, negative energy states in the Dirac sea must be included in the basis in terms of which nucleon wave functions are expanded. We studied in detail the effects and contributions of negative energy states. Without negative energy levels included, the calculated nuclear properties depend on the initial potentials very much. A small component from negative energy states in the wave functions, about 10^{-4} to 10^{-5}, contributes to the physical observables, such as E/A and r_{rms}, by the magnitude of 1–10%. When the initial potentials differ more from the converged ones, the contribution from negative energy levels becomes more important.

We conclude that the Woods-Saxon basis provides a compromise between the harmonic oscillator basis and the coordinate space, which may be used to describe exotic nuclei both properly and efficiently.

The extension of the relativistic Hartree theory in the Woods-Saxon basis to deformed cases with pairing correlations included is in progress.

ACKNOWLEDGMENTS

The authors thank Roger Hilton for a careful reading of the manuscript. S.G.Z. acknowledges the Max-Planck-Institut für Kernphysik for kind hospitality where part of this work was done. J.M. acknowledges the Physikdepartment, Technische Universität München for kind hospitality. This work was partly supported by the Major State Basic Research Development Program under Contract No. G2000077407, the National Natural Science Foundation of China under Grant Nos. 10025522, 10047001, 10221003, and 19935030, and the Bundesministerium für Bildung und Forschung under Project No. 06 MT 193.

[1] M.G. Mayer and J.H.D. Jensen, *Elementary Theory of Nuclear Shell Struture* (Wiley, New York, 1955).
[2] A. Bohr and B.R. Mottelson, *Nuclear Structure* (Benjamin, New York, 1969), Vol. I.
[3] P. Ring and P. Schuck, *The Nuclear Many-Body Problem* (Springer-Verlag, Berlin, 1980).
[4] R.D. Woods and D.S. Saxon, Phys. Rev. **95**, 577 (1954).
[5] S.G. Nilsson, K. Dan. Vidensk. Selsk. Mat. Fys. Medd. **29**, 16 (1955).
[6] J. Dobaczewski, W. Nazarewicz, T.R. Werner, J.-F. Berger, C.R. Chinn, and J. Dechargé, Phys. Rev. C **53**, 2809 (1996).
[7] J. Meng and P. Ring, Phys. Rev. Lett. **77**, 3963 (1996); J. Meng, Nucl. Phys. **A635**, 3 (1998); J. Meng and P. Ring, Phys. Rev. Lett. **80**, 460 (1998).
[8] S.-G. Zhou, J. Meng, S. Yamaji, and S.C. Yang, Chin. Phys. Lett. **17**, 717 (2000).
[9] M.V. Stoitsov, P. Ring, D. Vretenar, and G.A. Lalazissis, Phys. Rev. C **58**, 2086 (1998); M.V. Stoitsov, W. Nazarewicz, and S. Pittel, *ibid.* **58**, 2092 (1998).
[10] J. Dobaczewski, H. Flocard, and J. Treiner, Nucl. Phys. **A422**, 103 (1984).
[11] J. Terasaki, P.-H. Heenen, H. Flocard, and P. Bonche, Nucl. Phys. **A600**, 371 (1996); J. Terasaki, H. Flocard, P.-H. Heenen, and P. Bonche, *ibid.* **A621**, 706 (1997).
[12] W. Pöschl, D. Vretenar, G.A. Lalazissis, and P. Ring, Phys. Rev. Lett. **79**, 3841 (1997).
[13] S.T. Belyaev, A.V. Smirnov, S.V. Tolokonnikov, and S.A. Fayans, Yad. Fiz. **45**, 1263 (1987) [Sov. J. Nucl. Phys. **45**, 783 (1987)].
[14] P.-G. Reinhard, M. Bender, K. Rutz, and J.A. Maruhn, Z. Phys. A **358**, 277 (1997).
[15] W. Pöschl, Comput. Phys. Commun. **112**, 42 (1998).
[16] V. E. Oberacker and A. S. Umar, *Proceedings of the International Symposium on Perspectives in Nuclear Physics* (World Scientific, Singapore, 1999).

[17] W.H. Press, S.A. Teukolsky, W.T. Vetterling, and B.P. Flannery, *Numerical Recipes in Fortran 77*, 2nd ed. (Cambridge University Press, Cambridge, 1992).
[18] B.D. Serot and J.D. Walecka, Adv. Nucl. Phys. **16**, 1 (1986).
[19] P.-G. Reinhard, Rep. Prog. Phys. **52**, 439 (1989).
[20] P. Ring, Prog. Part. Nucl. Phys. **37**, 193 (1996); **46**, 165 (2001).
[21] J. Boguta and A.R. Bodmer, Nucl. Phys. **A292**, 413 (1977).
[22] C.J. Horowitz and B.D. Serot, Nucl. Phys. **A368**, 503 (1981).
[23] Y.K. Gambhir, P. Ring, and A. Thimet, Ann. Phys. (N.Y.) **198**, 132 (1990).
[24] W. Koepf and P. Ring, Z. Phys. A **339**, 81 (1991).
[25] K. Heyde, *Basis Ideas and Concepts in Nuclear Physics*, 2nd ed. (IOP, Bristol, 1999).
[26] G. Audi and A.H. Wapstra, Nucl. Phys. **A595**, 409 (1995).
[27] H. De Vries, C.W. De Jager, and C. De Vries, At. Data Nucl. Data Tables **36**, 495 (1987).
[28] S. Im and J. Meng, Phys. Rev. C **61**, 047302 (2000).
[29] I. Hamamoto, H. Sagawa, and X.Z. Zhang, Phys. Rev. C **64**, 024313 (2001).
[30] S.-Q. Zhang, J. Meng, S.-G. Zhou, and J.-Y. Zeng, Chin. Phys. Lett. **19**, 312 (2002).
[31] J. Meng, H. Toki, J.Y. Zeng, S.Q. Zhang, and S.-G. Zhou, Phys. Rev. C **65**, 041302(R) (2002).